

Comparison of model predictions for the composition of the ionosphere of Mars to MAVEN NGIMS data

Paul Withers, Marissa Vogt, Majd Mayyasi, Paul Mahaffy, Mehdi Benna, Meredith Elrod, Stephen Bougher, Chuanfei Dong, Jean-Yves Chaufray, Yingjuan Ma, et al.

▶ **To cite this version:**

Paul Withers, Marissa Vogt, Majd Mayyasi, Paul Mahaffy, Mehdi Benna, et al.. Comparison of model predictions for the composition of the ionosphere of Mars to MAVEN NGIMS data. Geophysical Research Letters, 2015, 42 (21), pp.8966-8976. 10.1002/2015GL065205 . insu-01238399

HAL Id: insu-01238399
https://insu.hal.science/insu-01238399

Submitted on 6 Aug 2020

HAL is a multi-disciplinary open access archive for the deposit and dissemination of scientific research documents, whether they are published or not. The documents may come from teaching and research institutions in France or abroad, or from public or private research centers.

L'archive ouverte pluridisciplinaire **HAL**, est destinée au dépôt et à la diffusion de documents scientifiques de niveau recherche, publiés ou non, émanant des établissements d'enseignement et de recherche français ou étrangers, des laboratoires publics ou privés.

AGU PUBLICATIONS

Geophysical Research Letters

RESEARCH LETTER
10.1002/2015GL065205

Special Section:
First Results from the MAVEN Mission to Mars

Comparison of model predictions for the composition of the ionosphere of Mars to MAVEN NGIMS data

Paul Withers[1,2], Marissa Vogt[2], Majd Mayyasi[2], Paul Mahaffy[3], Mehdi Benna[3], Meredith Elrod[3], Stephen Bougher[4], Chuanfei Dong[4], Jean-Yves Chaufray[5], Yingjuan Ma[6], and Bruce Jakosky[7]

[1]Department of Astronomy, Boston University, Boston, Massachusetts, USA, [2]Center for Space Physics, Boston University, Boston, Massachusetts, USA, [3]Planetary Environments Laboratory, NASA Goddard Space Flight Center, Greenbelt, Maryland, USA, [4]Atmospheric, Oceanic and Space Sciences Department, University of Michigan, Ann Arbor, Michigan, USA, [5]Laboratoire Atmosphère, Milieux et Observations Spatiales, Institut Pierre-Simon Laplace, Paris, France, [6]Institute of Geophysics and Planetary Physics, University of California, Los Angeles, California, USA, [7]Laboratory for Atmospheric and Space Physics, University of Colorado Boulder, Boulder, Colorado, USA

Abstract Prior to the arrival of the Mars Atmosphere and Volatile EvolutioN (MAVEN) spacecraft at Mars, the only available measurements of the composition of the planet's ionosphere were those acquired by the two Viking Landers during their atmospheric entries. Many numerical models of the composition of the ionosphere of Mars have been developed, but these have only been validated for species, altitudes, and conditions for which Viking data exist. Here we compare the ionospheric composition and structure predicted by 10 ionospheric models at solar zenith angles of 45–60° against ion density measurements acquired by the MAVEN Neutral Gas and Ion Mass Spectrometer (NGIMS). The most successful models included three-dimensional plasma transport driven by interactions with the surrounding space environment but had relatively simple ionospheric chemistry.

Key Points:
- Topside composition is mixture of O^+ and O_2^+
- Few models predict topside composition accurately
- Most successful models simulated interactions with surrounding space environment

Correspondence to:
P. Withers,
withers@bu.edu

Citation:
Withers, P., et al. (2015), Comparison of model predictions for the composition of the ionosphere of Mars to MAVEN NGIMS data, *Geophys. Res. Lett.*, *42*, 8966–8976, doi:10.1002/2015GL065205.

Received 2 JUL 2015
Accepted 20 AUG 2015
Published online 5 NOV 2015

©2015. American Geophysical Union. All Rights Reserved.

1. Introduction

For almost four decades, only two vertical profiles of the composition of the ionosphere of Mars have been available for study. Those profiles were measured by Viking Landers 1 and 2 during their descents to the surface of Mars on 20 July 1976 (solar longitude (Ls) = 97°) and 3 September 1976 (Ls = 118°), respectively. Both profiles were measured by the retarding potential analyzer (RPA) instrument at solar zenith angles near 45° during solar minimum conditions (the solar 10.7 cm radio flux, $F_{10.7}$, at Earth ≈70) and near aphelion. Analysis of raw RPA data required the Viking investigators to specify the chemical constituents of the ionosphere before ion densities could be inferred by fitting the raw data [*Hanson et al.*, 1977]. The preferred analysis included only O^+, O_2^+, and CO_2^+ ions, although the data could also have been consistent with the presence of NO^+, CO^+, and N_2^+ [*Hanson et al.*, 1977]. The Viking lander ion composition data shown in Figure 6 of *Hanson et al.* [1977] extend from 120 km to almost 300 km with a vertical resolution of 5 km. The minimum reported ion density was on the order of 100 cm^{-3}. The main features of the Viking profiles are as follows:

1. Between 125 km and 225 km, the ratio of CO_2^+ density to O_2^+ density is practically constant (0.13 ± 0.02).
2. O_2^+ is the dominant ion species at all altitudes measured.
3. O^+ is more abundant than CO_2^+ above 210 km.
4. The peak O^+ abundance of 700 cm^{-3} occurs at 230 km.
5. In the Viking Lander 1 profile, the O_2^+ and CO_2^+ densities decrease exponentially with increasing altitude from shortly above the ionospheric peak to the top of the profiles (290 km for O_2^+ and 230 km for CO_2^+). Between 150 km and 280 km, the O_2^+ scale height is 26 km. Between 150 km and 220 km, the CO_2^+ scale height is 22 km.
6. In the Viking Lander 2 profile, the O_2^+ and CO_2^+ densities decrease with increasing altitude above the peak, but both have a noticeable increase in scale height above 180 km.

Since the Viking landings, these ion composition data have been used as benchmarks for every model of the ionosphere of Mars. In turn, these models have predicted ionospheric conditions at altitudes, solar zenith angles, and solar activities not sampled by the Viking Landers. The chemical composition of the ionosphere is critically important for every aspect of ionospheric behavior, including dynamics, energetics,

electrodynamics, interactions with the neutral atmosphere, interactions with the surrounding plasma environment, and the escape of volatiles. It is therefore important to test the many models of ionospheric composition that have been introduced since those Viking observations were made. Although most published models reproduce the Viking observations adequately, these models make a wide range of predictions concerning species and altitudes not observed by the Viking Landers. Evaluation of which predictions are good and which are not good will identify which models are most realistic. More significantly, comparison of the assumptions underlying these models has the potential to quickly indicate where assumptions are poor. For instance, if all successful models include a given set of chemical reactions, but all unsuccessful models do not, then it can be concluded that this set of chemical reactions is significant for the ionosphere of Mars.

The aim of this article is to evaluate previously published ion composition predictions made by numerical models. This aim will be achieved by comparison of ion compositions predicted by models and observed by Mars Atmosphere and Volatile EvolutioN (MAVEN) Neutral Gas and Ion Mass Spectrometer (NGIMS). To the extent possible, the observations are compared to predictions made using a similar solar irradiance and heliocentric distance. The consequences of differences between modeled and observed conditions are discussed later.

Section 2 describes the MAVEN NGIMS data that are used in this work, section 3 presents the predictions of 10 ionospheric models and compares them to the MAVEN NGIMS data, and section 4 summarizes the conclusions of this work.

2. MAVEN NGIMS Observations of Ionospheric Composition

The MAVEN spacecraft has been orbiting Mars since 22 September 2014. On each 4.6 h elliptical orbit, the spacecraft dips into the upper atmosphere and ionosphere as it descends to and ascends from its periapsis. Periapsis altitude is typically 150 km but can be as low as 120 km during occasional "deep dip campaigns." During many periapsis passes, the MAVEN ion/neutral mass spectrometer, NGIMS, makes in situ measurements of the composition of the ionosphere below 500 km [*Mahaffy et al.*, 2014]. NGIMS, which is the latest in a long series of successful spacecraft mass spectrometers from the NASA Goddard Space Flight Center, makes these measurements using a dual ion source and a quadrupole analyzer. It has unit mass resolution over its full range of 2 to 150 amu, and its vertical resolution is much less than the neutral scale height. For the period analyzed here (February 2015 to May 2015, Ls = 299°–348° of Mars Year 32), solar activity was moderate ($F_{10.7}$ at Earth ≈140) and the planet was near perihelion (1.42–1.53 AU). One hundred and two orbits of data are used that cover latitudes 60°S–40°N and local solar times 8–16 h.

We consider all MAVEN NGIMS measurements of the density of the following ion masses: 12 (C^+), 16 (O^+), 17 (OH^+), 28 (N_2^+, CO^+), 29 (HCO^+, N_2H^+), 30 (NO^+), 31 (HNO^+), 32 (O_2^+), 33 (HO_2^+), and 44 (CO_2^+). The Viking Lander observations and all model output discussed in section 3 are at solar zenith angles of either 45° or 60°. Since *Benna et al.* [2015] showed that variations in ionospheric composition and density are relatively small over that range, for each ion mass, we select all measurements between 45 and 60° solar zenith angle. We further divide these measurements into 10 km vertical bins. For each ion mass and each 10 km vertical bin, we find the median ion density and report the resultant profiles in Figure 1. The formal 1σ uncertainty in an individual MAVEN NGIMS density measurement is 20%. Since some of the contributions to that uncertainty are systematic, not random, a similar uncertainty should be assigned to the median densities reported here. Furthermore, MAVEN NGIMS ion densities are calibrated by normalizing the sum of the count rate of all ions to the electron density measured by the Langmuir Probe and Waves instrument. This calibration was performed in the first few weeks of the mission [*Benna et al.*, 2015], and the possibility of drifts in the calibration is still being assessed. The main features of these MAVEN NGIMS ion density profiles are as follows:

1. Between 200 km and 400 km, the ratio of CO_2^+ density to O_2^+ density decreases exponentially with altitude from 0.08 at 200 km to 0.02 at 400 km with a scale height of 155 km.
2. Below 290 km, O_2^+ is the dominant ion species. Above 290 km, O_2^+ and O^+ have roughly equal densities.
3. O^+ is more abundant than CO_2^+ above 220 km.
4. The peak O^+ abundance of 1500 cm^{-3} occurs at 300 km.
5. O_2^+ and CO_2^+ densities decrease exponentially with increasing altitude above the peak. Between 180 km and 330 km, the O_2^+ scale height is 44 km, and the CO_2^+ scale height is 34 km.

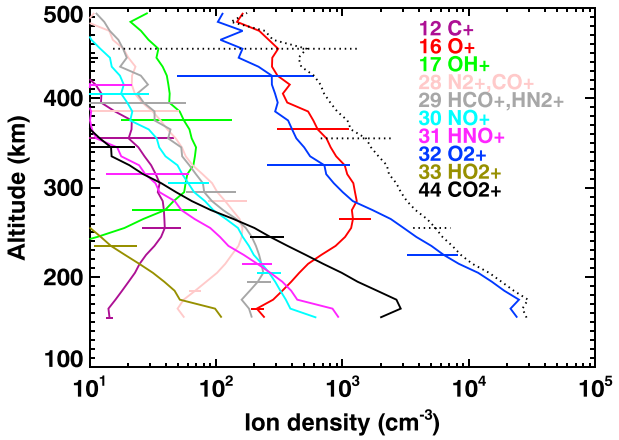


Figure 1. Median MAVEN NGIMS ion density profiles for solar zenith angles of 45°–60°. Species are indicated by color: mass 12 (C^+) in purple, mass 16 (O^+) in red, mass 17 (OH^+) in light green, mass 28 (N_2^+, CO^+) in salmon pink, mass 29 (HCO^+, N_2H^+) in grey, mass 30 (NO^+) in cyan, mass 31 (HNO^+) in magenta, mass 32 (O_2^+) in blue, mass 33 (HO_2^+) in olive green, and mass 44 (CO_2^+) in black. The total ion density is shown by the dashed black line. Horizontal lines show lower and upper quartile ranges.

6. Between 160 km and its peak at 300 km, the O^+ density increases exponentially with increasing altitude with a scale height of 55 km. The scale height for the increase in O^+ density (55 km) is quite similar to the scale height for the decrease in O_2^+ density (44 km).

In addition to these main features, we also note that mass 12 (C^+) peaks at 300 km and 5×10^1 cm^{-3}, mass 17 (OH^+) peaks at 330 km and 6×10^1 cm^{-3}, mass 28 (N_2^+, CO^+) peaks at 270 km and 170 cm^{-3}, mass 29 (HCO^+, N_2H^+) peaks at 210 km and 240 cm^{-3}, mass 30 (NO^+) decreases exponentially with altitude with a scale height of 75 km and density of 160 cm^{-3} at 250 km, mass 31 (HNO^+) decreases exponentially with altitude with a scale height similar to that of CO_2^+ and density of 100 cm^{-3} at 250 km, and mass 33 (HO_2^+) decreases exponentially with altitude with a scale height similar to that of CO_2^+ and density of 10 cm^{-3} at 250 km. Some of these key features are tabulated in Table 1 alongside the relevant predictions of various models. Since all models discussed here that include both mass 29 ions, HCO^+ and N_2H^+, predict that the HCO^+ density is much greater than the N_2H^+ density, the analysis in section 3 assumes that all observed mass 29 ions are HCO^+.

3. Model Predictions of Ionospheric Composition

The chemical composition of the ionosphere of Mars has been simulated by many workers, including *Chen et al.* [1978], *Shinagawa and Cravens* [1992], *Krasnopolsky* [2002], *Ma et al.* [2004], *Terada et al.* [2009],

Table 1. Key Features of Observed and Predicted Ion Density Profiles[a]

Feature	VL1	NGIMS	C78	S92	K02	M04	T09	N11	M14	C14	F15	D15
Solar activity	Min	Mod	Min	Min	Mod	Min	Min	Min	Min	Mod	Min	Min
Dominant ion species at 300 km and above	O_2^+	O^+, O_2^+	O_2^+	O^+	O_2^+	O^+, O_2^+	O^+	O_2^+	O_2^+	N/A	O_2^+	O^+, O_2^+
Does O^+ have a single scale height from 150 km to peak?	Yes	Yes	Yes	No	Yes, but	Yes	No	Yes	Yes	Yes, but	Yes, but	No
O^+ peak altitude (km)	230	300	220	260	210	230	250	230	240	220	220	220
O^+ peak density (cm^{-3})	7×10^2	1.5×10^3	6×10^2	1.5×10^3	3×10^2	4×10^2	2×10^3	2×10^2	3×10^2	2×10^3	7×10^2	8×10^2
$O^+ = CO_2^+$ altitude (km)	210	220	210	210	N/A	210	210	230	240	190	220	200
$O^+ = CO_2^+$ density (cm^{-3})	6×10^2	6×10^2	4×10^2	4×10^2	N/A	3×10^2	3×10^2	2×10^2	3×10^2	2×10^3	7×10^2	5×10^2

[a]VL1 is Viking Lander 1 [*Hanson et al.*, 1977], C78 is *Chen et al.* [1978], S92 is *Shinagawa and Cravens* [1992], K02 is *Krasnopolsky* [2002], M04 is *Ma et al.* [2004], T09 is *Terada et al.* [2009], N11 is *Najib et al.* [2011], M14 is *Matta et al.* [2014], C14 is *Chaufray et al.* [2014], F15 is *Fox* [2015], and D15 is *Dong et al.* [2015]. Solar activity is either "Mod" (moderate) or "Min" (minimum). For the O^+ scale height, "Yes, but" means that although the O^+ density does change exponentially, its scale height is not similar to the O_2^+ scale height. "$O^+ = CO_2^+$" refers to the location at which O^+ and CO_2^+ densities are equal.

Najib et al. [2011], *Matta et al.* [2014], *Chaufray et al.* [2014], *Fox* [2015], and *Dong et al.* [2015]. In this section, we compare published predictions made for solar zenith angles of 45° to 60° and solar minimum to moderate conditions to MAVEN NGIMS data acquired at solar zenith angles of 45° to 60° and solar moderate conditions (Figure 1). These published predictions correspond to heliocentric distances between the semimajor axis and aphelion, whereas the observations correspond to heliocentric distances near perihelion. Where modelers have reported the results of simulations from a given model in a series of papers, we concentrate on the most recently reported set of suitable ion density profiles.

Chen et al. [1978] developed a one-dimensional model of ionospheric photochemistry, vertical dynamics, and energetics between 100 km and 360 km in order to reproduce the Viking Lander 1 ion density measurements. The model included H^+, O^+, NO^+, O_2^+, and CO_2^+ ion species. They reported ion density profiles for Viking-like solar activity and solar zenith angle, which are shown in Figure 2a (their Figure 6). In this model, NO^+, CO_2^+, and O_2^+ ion densities decrease exponentially with altitude with scale heights of 33 km, 23 km, and 33 km, respectively, up to 270 km. Above 270 km, the scale heights for O_2^+ and CO_2^+ become significantly larger. By contrast, in the MAVEN NGIMS profiles, the densities of these three species continue to decrease exponentially with altitude to much higher altitudes, and the O_2^+ and CO_2^+ scale heights do not become significantly larger above 270 km. Unlike in the MAVEN NGIMS profiles, where O^+ and O_2^+ densities are approximately equal above 290 km, the O^+ density is always less than the O_2^+ density, being at most 40% of the O_2^+ density. The O^+ density increases exponentially with altitude from 150 km up to its peak with a scale height that is similar to the scale height for the decrease in the O_2^+ density with altitude, behavior that is similar to that seen in the MAVEN NGIMS profile. The O^+ peak density is 6×10^2 cm^{-3} at 220 km, much smaller and at lower altitude than in the MAVEN NGIMS profiles. Similarly to the MAVEN NGIMS observations, the O^+ and CO_2^+ densities are equal at 210 km and 4×10^2 cm^{-3}. The NO^+ density at 200 km is smaller than the MAVEN NGIMS NO^+ density at this altitude, and its scale height of 33 km is much smaller than the corresponding MAVEN NGIMS scale height of 100 km. The solar cycle is probably responsible for some of these differences, but it is unlikely to explain the differences that concern the shift in O_2^+ and CO_2^+ scale heights at 270 km or the dominant ion species at high altitudes.

Shinagawa and Cravens [1992] discussed a one-dimensional multispecies magnetohydrodynamic (MHD) model of the ionosphere of Mars (100–400 km). The model included H^+, O^+, O_2^+, and CO_2^+ ion species. They used this model to study the effects on the ionosphere of magnetic fields induced by magnetospheric interactions and imposed by an intrinsic planetary field in order to investigate if the question of whether Mars has an intrinsic magnetic field could be resolved by analysis of observations of the structure of the ionosphere. They conducted several simulations with different assumptions for the magnetic environment under the conditions of the Viking Lander 1 ionospheric measurements: solar minimum and a solar zenith angle of 44°. One of the two sets of ion density profiles they reported is shown in Figure 2b (their Figure 10); the other set is similar. In this model, the O_2^+ density decreases exponentially with altitude from the peak to the top of the simulation at 400 km. By contrast, the CO_2^+ density decreases exponentially with altitude with a similar scale height until 230 km, above which it is practically uniform. The MAVEN NGIMS profiles do not show this behavior for CO_2^+, nor do they show O^+ being the dominant ion species above 260 km. The simulated O^+ density increases with altitude from 150 km to its peak of 1.5×10^3 cm^{-3} at 260 km, but this increase is not a steady exponential. Instead, unlike the MAVEN NGIMS observations, the O^+ density profile contains a significant inflection at 210 km. Unlike in the MAVEN NGIMS profiles, where O^+ and O_2^+ densities are approximately equal above 290 km, the O^+ density is significantly greater than the O_2^+ density above 250 km. Similarly to the MAVEN NGIMS observations, the O^+ and CO_2^+ densities are equal at 210 km and 4×10^2 cm^{-3}. Solar cycle differences are unlikely to account for the differences that concern the behavior of CO_2^+ at high altitudes, the inflection in the O^+ density profile at 210 km, or the dominant ion species at high altitudes. An earlier version of this model [*Shinagawa and Cravens*, 1989] explored five different sets of assumptions for the magnetic field and plasma transport: four of them resulted in CO_2^+ behavior similar to *Shinagawa and Cravens* [1992]. The other did reproduce an exponential decrease in CO_2^+ density with increasing altitude but predicted much too high densities at high altitudes.

Krasnopolsky [2002] developed a one-dimensional model of the thermosphere and ionosphere (80–300 km) in order to explore the fractionation of escaping hydrogen and the implications of the current D/H ratio for the past water inventory of Mars. The model included 18 ion species. H^+, H_2^+, He^+, C^+, N^+, O^+, N_2^+, CO^+, CO_2^+, and Ar^+ were produced by photoionization, whereas OH^+, NH^+, HN_2^+, ArH^+, O_2^+, NO^+, HCO^+, and HCO_2^+ were produced by subsequent ion-neutral reactions. Ion density profiles at 60° solar zenith angle were reported

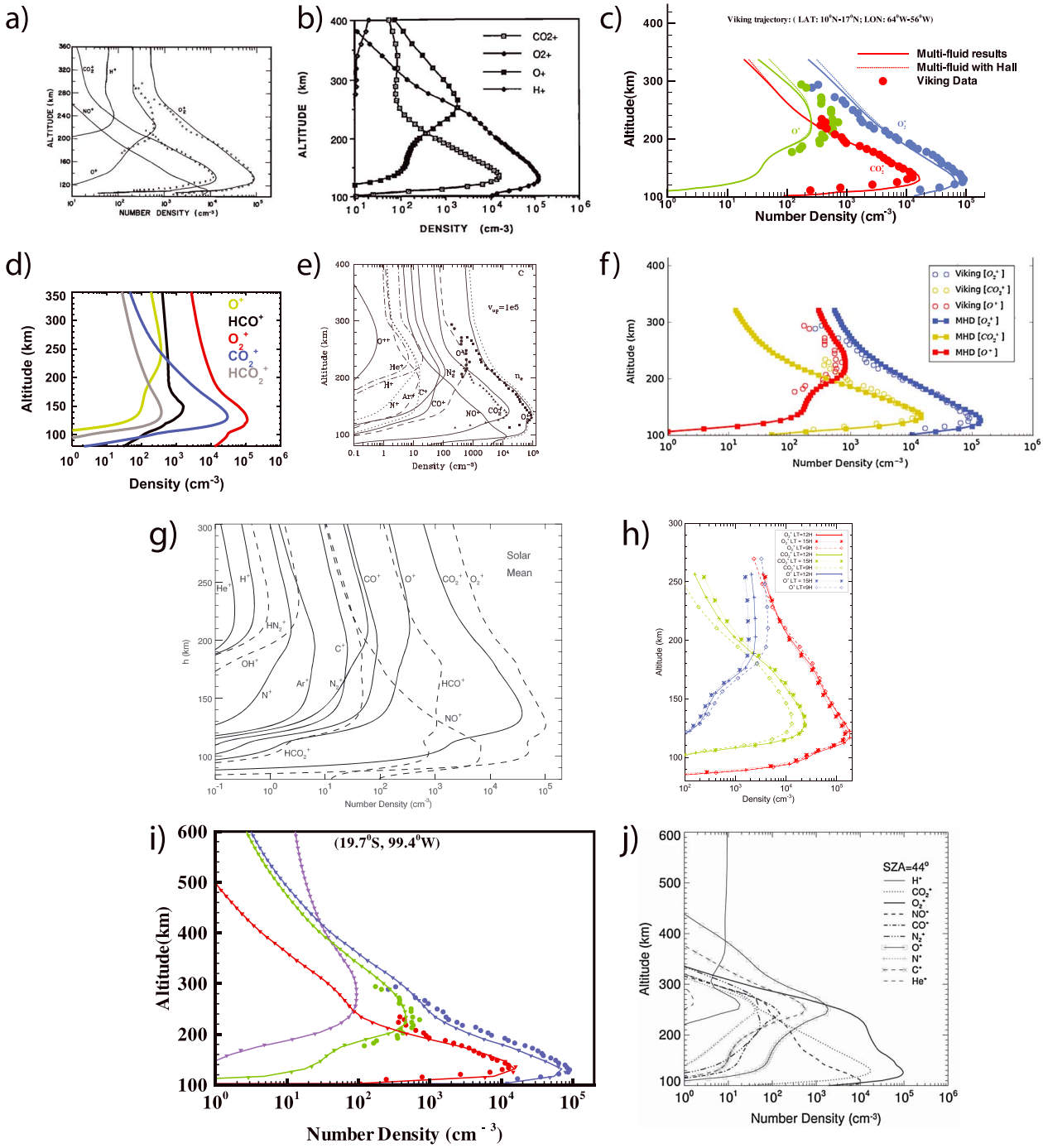


Figure 2. Ten sets of simulated ion density profiles. (a) Figure 6 of *Chen et al.* [1978]. (b) Figure 10 of *Shinagawa and Cravens* [1992]. (c) Figure 8 of *Najib et al.* [2011]. (d) Figure 9a of *Matta et al.* [2014]. (e) Figure 4c of *Fox* [2015]. (f) *Dong et al.* [2015]. (g) Figure 2 of *Krasnopolsky* [2002]. (h) Figure 4a of *Chaufray et al.* [2014]. O^+ is in blue, O_2^+ is in red, and CO_2^+ is in green. The text focuses on the simulation for 15 h local time, the results of which are shown with asterisks and dotted lines. Dashed lines and diamonds correspond to the simulation for 9 h local time, and solid lines and crosses correspond to the simulation for 12 h local time. (i) Figure 8 of *Ma et al.* [2004]. H^+ is in lavender, O^+ is in green, O_2^+ is in blue, and CO_2^+ is in red. (j) Figure 3 of *Terada et al.* [2009]. Figures are reproduced by permission of the respective publishers. See the original publications for larger symbols and labels and more complete captions.

for solar minimum, moderate, and maximum conditions. The solar moderate ion density profiles are shown in Figure 2g (their Figure 2). In this model, densities of O_2^+ and CO_2^+ decrease exponentially with altitude up to the top of the model at 300 km. However, the ratio of CO_2^+ to O_2^+ density is approximately 3 times larger in the model than in the MAVEN NGIMS observations. Even near the O^+ peak density of 3×10^2 cm^{-3} at 210 km, the O^+ density is always much less than the O_2^+ density, being at most 10% of the O_2^+ density. In the MAVEN NGIMS observations, O^+ and O_2^+ densities are much more similar at 200–300 km. They are identical at 290 km and are within a factor of 2 of each other over the adjacent few scale heights. Although the O^+ density increases exponentially with altitude from 140 km up to its peak, its scale height is significantly larger than the scale height for the decrease in the O_2^+ density with altitude. In the model, the O^+ density is never greater than 20% of the CO_2^+ density, in stark contrast to the MAVEN NGIMS observations in which the O^+ density is an order of magnitude greater than the CO_2^+ density at 300 km. Although the NO^+ density decreases exponentially with altitude with similar scale heights in this model and the MAVEN NGIMS observations, the NO^+ density is an order of magnitude smaller in the model. In both the model and MAVEN NGIMS observations, the HCO^+ density decreases exponentially with altitude above its peak to a density of 1×10^2 cm^{-3} at 300 km. However, conditions at the HCO^+ peak differ slightly, being 180 km and 1×10^3 cm^{-3} in the model and 210 km and $2 - 3 \times 10^2$ cm^{-3} in the MAVEN NGIMS observations. Since this simulation was conducted under solar moderate conditions similar to those experienced by MAVEN NGIMS, model-observation differences cannot be attributed to the solar cycle. The differences in the behavior of O^+, CO_2^+, and NO^+ are substantial.

Ma et al. [2004] discussed a three-dimensional multispecies MHD model of the ionosphere of Mars and surrounding space environment. The model included H^+, O^+, O_2^+, and CO_2^+ ion species. They used this model to explore the interaction of the solar wind with the magnetosphere and ionosphere of Mars, including the effects of the planet's crustal magnetic fields. They simulated Viking-like solar minimum conditions and reported ion density profiles (100–600 km) for the location of the Viking Lander 1 entry, the subsolar point, and locations 45° north and south of the subsolar point. Figure 2i shows the profile simulated 45° south of the subsolar point (their Figure 8). In this model, O_2^+ and CO_2^+ ion densities decrease exponentially with altitude with similar scale heights up to 240 km. Above 240 km, they decrease exponentially with altitude with larger scale heights. This shift in scale height at 240 km is not present in the MAVEN NGIMS observations. The densities of O^+ and O_2^+ are very similar above 280 km, as in the MAVEN NGIMS observations. The O^+ density increases exponentially with altitude from 150 km up to its peak with a scale height that is similar to the scale height for the decrease in the O_2^+ density with altitude, behavior that is similar to that seen in the MAVEN NGIMS profile. The O^+ peak density is 4×10^2 cm^{-3} at 230 km, much smaller and at lower altitude than in the MAVEN NGIMS profiles. Similarly to the MAVEN NGIMS observations, the O^+ and CO_2^+ densities are equal at 210 km and 3×10^2 cm^{-3}. The only significant difference between model prediction and MAVEN NGIMS observations, the O^+ peak, is likely caused by differences in solar activity. However, that is only true for the model prediction 45° south of the subsolar point. The profile from 45° north of the subsolar point has all ion densities less than 1×10^2 cm^{-3} above 300 km [*Ma et al.*, 2004], an order of magnitude smaller than the MAVEN NGIMS densities.

Terada et al. [2009] developed a three-dimensional global MHD model of the interaction between the solar wind and the ionosphere of Mars. The model included CO_2^+, O_2^+, NO^+, CO^+, N_2^+, O^+, N^+, C^+, He^+, and H^+ ion species. They used this model to explore the plasma environment of early Mars under extreme solar wind and extreme ionizing irradiance conditions. In order to validate the model for studies of early Mars, they simulated Viking-like solar minimum conditions and reported ion density profiles for the location of the Viking Lander 1 entry, as shown in Figure 2j (their Figure 3). In this model, the O_2^+ density decreases exponentially with altitude from the peak to 230 km. Above 230 km, the O_2^+ scale height becomes significantly smaller. By contrast, the CO_2^+ scale height is uniform up to above 300 km. This shift in the O_2^+ scale height at 230 km is not present in the MAVEN NGIMS observations. The simulated O^+ density increases with altitude from 150 km to its peak of 2×10^3 cm^{-3} at 250 km, but this increase is not a steady exponential. Instead, unlike the MAVEN NGIMS observations, the O^+ density profile contains a significant inflection at 190 km. Unlike in the MAVEN NGIMS profiles, where O^+ and O_2^+ densities are approximately equal above 290 km, the O^+ density is significantly greater than the O_2^+ density above 260 km. Similarly to the MAVEN NGIMS observations, the O^+ and CO_2^+ densities are equal at 210 km and 3×10^2 cm^{-3}. The NO^+ density decreases roughly exponentially with altitude up to above 300 km, similar behavior to that seen by MAVEN NGIMS. The model and observations have the same NO^+ density at 200 km, 3×10^2 cm^{-3}. The model's NO^+ scale height is much smaller than the NO^+ scale height in the MAVEN NGIMS observations. In the model, the two mass 28 species, N_2^+ and CO^+,

have similar vertical profiles, which makes comparison to MAVEN NGIMS observations of mass 28 ions possible. In both the model and the MAVEN NGIMS observations, the density of mass 28 ions increases exponentially with altitude until a peak then decreases exponentially with altitude above that peak. Peak density for mass 28 ions occurs around 100–200 cm^{-3} and 240 km in the model and 170 cm^{-3} and 270 km in the MAVEN NGIMS observations. Solar cycle differences are unlikely to account for the differences that concern the inflection in the O^+ density profile at 190 km, the inflection in the O_2^+ density profile at 230 km, or the dominant ion species at high altitudes.

Najib et al. [2011] developed a multifluid version of the model used by *Ma et al.* [2004]. Separate mass, momentum, and energy equations were solved for each of the four ion species: H^+, O^+, O_2^+, and CO_2^+. In other respects, these simulations were similar to those of *Ma et al.* [2004]. Ion density profiles were reported for Viking-like conditions of solar minimum and 44° solar zenith angles between 100 km and 340 km, as shown in Figure 2c (their Figure 8). In this model, O_2^+ and CO_2^+ ion densities decrease exponentially with altitude with similar scale heights up to 340 km. Unlike in the MAVEN NGIMS profiles, where O^+ and O_2^+ densities are approximately equal above 290 km, the O^+ density is always less than the O_2^+ density, being at most 20% of the O_2^+ density. The O^+ density increases exponentially with altitude from 160 km up to its peak with a scale height that is similar to the scale height for the decrease in the O_2^+ density with altitude, behavior that is similar to that seen in the MAVEN NGIMS profile. The O^+ peak density is 2×10^2 cm^{-3} at 230 km, much smaller and at lower altitude than in the MAVEN NGIMS profiles. Similarly to the MAVEN NGIMS observations, the O^+ and CO_2^+ densities are equal at 230 km and 2.5×10^2 cm^{-3}. Solar cycle differences are unlikely to account for the differences that concern the dominant ion species at high altitudes.

Matta et al. [2014] used a one-dimensional model (80–400 km) of ionospheric photochemistry and vertical dynamics to investigate the importance of self-consistent calculations of ion and electron temperature on predicted ionospheric conditions. The model included 16 ion species [*Matta et al.*, 2013]. H^+, H_2^+, O^+, N_2^+, CO^+, CO_2^+, and Ar^+ were produced by photoionization, whereas H_3^+, OH^+, NO^+, O_2^+, HCO^+, HOC^+, ArH^+, N_2H^+, and HCO_2^+ were produced by subsequent ion-neutral reactions. Ion density profiles at solar minimum and 47° solar zenith angle were reported for a subset of species (O^+, O_2^+, CO_2^+, HCO^+, and HCO_2^+) between 80 km and 350 km and are shown in Figure 2d (their Figure 9a). In this model, O_2^+ and CO_2^+ densities decrease exponentially with altitude up to the top of the model, but the scale height for the decrease in O_2^+ density is much larger than observed by MAVEN NGIMS. Unlike in the MAVEN NGIMS profiles, where O^+ and O_2^+ densities are approximately equal above 290 km, the dominant ion species at all altitudes is O_2^+. Indeed, the O^+ density never exceeds 10% of the O_2^+ density. The O^+ density increases exponentially with altitude from 170 km up to its peak with a scale height that is similar to the scale height for the decrease in the O_2^+ density with altitude, behavior that is similar to that seen in the MAVEN NGIMS profile. The O^+ peak density is 3×10^2 cm^{-3} at 240 km, much smaller and at lower altitude than in the MAVEN NGIMS profiles. The model predicts the HCO^+ density to be near constant at 5×10^2 cm^{-3} at all altitudes above 200 km, whereas the observed HCO^+ density decreases exponentially with altitude above its peak of 240 cm^{-3} at 210 km. Solar cycle differences are unlikely to account for the differences that concern the dominant ion species at high altitudes and the behavior of HCO^+.

Chaufray et al. [2014] added three-dimensional multifluid ionospheric dynamics to the photochemical ionospheric model of *González-Galindo et al.* [2013], which is incorporated within a general circulation model of the neutral atmosphere [*Forget et al.*, 1999]. The model included C^+, N^+, O^+, NO^+, O_2^+, and CO_2^+ ion species, although only O^+, O_2^+, and CO_2^+ were included in their figures of vertical profiles of ion density. They used this model to explore the effects on ionospheric composition and structure of three-dimensional plasma transport. They reported ion density profiles for moderate solar activity at solar zenith angles of 0 and 45° between 80 km and 250 km, shown in Figure 2h (their Figure 4). We focus on the set of profiles at 45° solar zenith angle (15h local time), but the other sets of profiles are quite similar. In this model, O_2^+ and CO_2^+ densities decrease exponentially with altitude up to the top of the model at 250 km. Although O_2^+ is the dominant ion species up to 250 km in both the model and MAVEN NGIMS observations, the O^+/O_2^+ ratio at this altitude is much larger in the model than in the MAVEN NGIMS observations. The O^+ peak density is 2×10^3 cm^{-3} at 220 km, similar in density, but lower in altitude than in the MAVEN NGIMS profiles. Although the O^+ density increases exponentially with altitude from 130 km up to its peak, its scale height is significantly smaller than the scale height for the decrease in the O_2^+ density with altitude. In the model, the O^+ and CO_2^+ densities are equal at 190 km and 2×10^3 cm^{-3}. By contrast, they are equal at 220 km and 6×10^2 cm^{-3} in the MAVEN NGIMS observations. This model's photochemical results for NO^+ were shown in *González-Galindo et al.* [2013] (their Figure 3).

The NO^+ density varied exponentially from 5×10^3 cm^{-3} at 110 km to 6×10^2 cm^{-3} at 200 km, larger than the densities seen by MAVEN NGIMS. Since this simulation was conducted under solar moderate conditions similar to those experienced by MAVEN NGIMS, model-observation differences cannot be attributed to the solar cycle. The most significant difference concerns the predicted O^+ density.

Fox [2015] used a longstanding one-dimensional model of ionospheric photochemistry and vertical dynamics to explore the chemistry of protonated species in the ionosphere (80–400 km). The model included 24 ion species (CO_2^+, Ar^+, N_2^+, several states of O^+, CO^+, C^+, N^+, O_2^+, NO^+, He^+, H^+, O^{2+}, H_2^+, HCO^+, $OCOH^+$, HO_2^+, OH^+, N_2H^+, H_3^+, HNO^+, ArH^+, and CH^+). Ion density profiles at 60° solar zenith angle were reported for solar minimum and maximum conditions. The solar minimum ion density profiles for a simulation with a specified upward ion flux are shown in Figure 2e (their Figure 4c). In this model, O_2^+ and CO_2^+ ion densities decrease exponentially with altitude above the peak until 230 km. Above 230 km, their scale heights increase. This shift in scale height at 230 km is not present in the MAVEN NGIMS observations. The ratio of CO_2^+ to O_2^+ density changes little with altitude, whereas it changes by a factor of 4 in the MAVEN NGIMS observations. Consequently, the CO_2^+/O_2^+ ratio at high altitudes is much greater in the model (0.1) than in the MAVEN NGIMS observations (0.02). Unlike in the MAVEN NGIMS profiles, where O^+ and O_2^+ densities are approximately equal above 290 km, the dominant ion species at all altitudes is O_2^+. The modeled O^+ density never exceeds 30% of the O_2^+ density. Although the O^+ density increases exponentially with altitude from 140 km up to its peak, its scale height is significantly larger than the scale height for the decrease in the O_2^+ density with altitude. The O^+ peak density is 7×10^2 cm^{-3} at 220 km, much smaller and at lower altitude than in the MAVEN NGIMS profiles. Similarly to the MAVEN NGIMS observations, the O^+ and CO_2^+ densities are equal at 220 km and 7×10^2 cm^{-3}. The NO^+ density decreases exponentially with altitude up to 240 km. Above 240 km, its scale height increases. By contrast, the MAVEN NGIMS NO^+ density decreases exponentially with altitude with a uniform scale height from 160 km to 400 km. The model's NO^+ scale height at 140–240 km is much smaller than the NO^+ scale height in the MAVEN NGIMS observations. HCO^+ ions are not shown in Figure 2e, although they are reported in Figure 4d of *Fox* [2015]. The peak HCO^+ density is 8×10^2 cm^{-3} at 190 km, which is larger in magnitude and lower in altitude than the peak observed by MAVEN NGIMS at 240 cm^{-3} and 210 km. In the model, the two mass 28 species, N_2^+ and CO^+, have similar vertical profiles, which makes comparison to MAVEN NGIMS observations of mass 28 ions possible. In both the model and the MAVEN NGIMS observations, the density of mass 28 ions increases exponentially with altitude until a peak then decreases exponentially with altitude above that peak. Peak density for mass 28 ions, the sum of N_2^+ and CO^+, occurs at 100–200 cm^{-3} and 210 km in the model and 200 cm^{-3} and 260 km in the MAVEN NGIMS observations. The solar cycle is probably responsible for some of these differences, but it is unlikely to explain the differences that concern the shift in O_2^+, CO_2^+, and NO^+ scale heights at 230 km, the small NO^+ scale height, or the dominant ion species at high altitudes.

Dong et al. [2015] extended the multifluid MHD model of *Najib et al.* [2011] by incorporating one-way coupling to two other comprehensive three-dimensional models in order to better simulate the interaction of the solar wind with the Mars upper atmosphere. Coupling to the M-GITM model provided neutral atmospheric properties and photoionization frequencies, while coupling to the M-AMPS model provided densities of hot oxygen atoms in the corona. As with *Najib et al.* [2011], separate continuity, momentum, and energy equations were solved for each of the four ion species: H^+, O^+, O_2^+, and CO_2^+. Ion density profiles were reported for solar minimum conditions and a solar zenith angle of 60° between 100 km and 320 km, as shown in Figure 2f. In this model, O_2^+ and CO_2^+ ion densities decrease exponentially with altitude with similar scale heights up to the top of the model. The densities of O^+ and O_2^+ are very similar above 280 km, as in the MAVEN NGIMS observations. The simulated O^+ density increases with altitude from 150 km to its peak of 800 cm^{-3} at 220 km, but this increase is not a steady exponential. Instead, unlike the MAVEN NGIMS observations, the O^+ density profile contains a significant inflection at 190 km. The O^+ peak density is 8×10^2 cm^{-3} at 220 km, somewhat smaller and at much lower altitude than in the MAVEN NGIMS profiles. Similarly to the MAVEN NGIMS observations, the O^+ and CO_2^+ densities are equal at 200 km and 5×10^2 cm^{-3}. The only significant difference between model prediction and MAVEN NGIMS observations, the O^+ peak, is likely caused by differences in solar activity.

4. Discussion and Conclusions

Few of the predictions discussed in this article used the same solar irradiance, heliocentric distance, and season as the MAVEN NGIMS observations. These differences may affect ionospheric composition and densities via their effects on neutral composition, neutral temperature, and electron and ion temperatures.

Nevertheless, several observed features of the composition and structure of the ionosphere were predicted accurately by most of the models highlighted in this article. These include (1) densities of CO_2^+ and O_2^+ are proportional over a wide range of altitudes, (2) densities of CO_2^+ and O_2^+ decrease exponentially with increasing altitude for 100 km above the main peak, (3) the O^+ density peaks at least 100 km above the peak densities of CO_2^+ and O_2^+, and (4) O_2^+ is the dominant species at altitudes below the O^+ peak. Furthermore, most of the models accurately predicted the altitude and density at which O^+ and CO_2^+ ion densities are equal.

In the MAVEN NGIMS observations, densities of O^+, O_2^+, and CO_2^+ all decrease exponentially with increasing altitude at high altitudes, specifically above 170 km for O_2^+ and CO_2^+ and above 300 km for O^+. Several models incorrectly predicted that ion densities would decrease slowly with increasing altitude at high altitudes. *Chen et al.* [1978] predicted scarcely any decrease in O^+ and O_2^+ density with increasing altitude above 270 km. *Shinagawa and Cravens* [1992] predicted scarcely any decrease in CO_2^+ density with increasing altitude above 230 km. *Terada et al.* [2009] predicted a shift in the O_2^+ scale height at 230 km. *Matta et al.* [2014] predicted only a factor of 3 decrease in O_2^+ density with increasing altitude from 200 km to 350 km. *Fox* [2015] predicted scarcely any decrease in O_2^+ and CO_2^+ density with increasing altitude above 250 km. Although the reported results of the model of *Chaufray et al.* [2014] did not extend to high enough altitudes for this issue to be a factor, extrapolation of their O^+ density profile beyond the top of their model suggests scarcely any decrease. By contrast, the results of *Ma et al.* [2004], *Najib et al.* [2011], and *Dong et al.* [2015] that are highlighted in this article do show exponential decreases at high altitudes similar to those observed. The highlighted results of *Ma et al.* [2004] were generated 45° south of the subsolar point. However, the results of *Ma et al.* [2004] that were generated 45° north of the subsolar point show ion densities at high altitudes that are much, much smaller than observed by MAVEN NGIMS. The MAVEN NGIMS data used in this article were collected both north and south of the subsolar point. A possible explanation for this set of outcomes is that interactions with the surrounding space environment are important for the structure of the topside ionosphere. This is indeed implied by the striking geographic variations in the simulation of *Ma et al.* [2004]. With the exception of *Ma et al.* [2004], *Terada et al.* [2009], *Najib et al.* [2011], and *Dong et al.* [2015], these existing ionospheric models do not include particularly sophisticated representations of the interactions of the thermosphere and ionosphere with the surrounding space environment. Solar wind erosion may be responsible for the differences between several predictions of slow decreases in the O_2^+ and CO_2^+ density with altitude and observations of more rapid decreases. The inhibiting effects of a horizontal magnetic field, either the crustal field or the draped interplanetary magnetic field, on the vertical transport of plasma, which lead to a reduced plasma scale height at high altitudes, may also be important [*Breus et al.*, 1998].

In the MAVEN NGIMS observations, the O^+ density peaked at 300 km and 1.5×10^3 cm^{-3}. Several models predicted O^+ peak density and peak altitude smaller and lower than the MAVEN NGIMS findings. However, for some of those models [*Chen et al.*, 1978; *Ma et al.*, 2004; *Terada et al.*, 2009; *Najib et al.*, 2011; *Matta et al.*, 2014; *Fox*, 2015; *Dong et al.*, 2015], these poor predictions for MAVEN NGIMS can be explained by the models using solar minimum conditions appropriate for Viking, not the solar moderate conditions appropriate for MAVEN NGIMS. This explanation is not possible for *Krasnopolsky* [2002], who predicted a small and low O^+ peak at solar moderate conditions. *Chaufray et al.* [2014] predicted an O^+ peak at solar moderate conditions with the right density but too low an altitude. *Ma et al.* [2004] also reported the results of a solar maximum simulation (their Figure 6). Here the O^+ peak density of 2×10^3 cm^{-3} occurred above 300 km. Assuming that the O^+ peak properties for solar moderate conditions lie somewhere between those for solar minimum and maximum conditions, it is likely that a solar moderate simulation using the model of *Ma et al.* [2004] would predict the O^+ peak density accurately but at a lower altitude than observed by MAVEN NGIMS. *Fox* [2015] also reported the results of a solar maximum simulation (their Figure 5). Here the O^+ peak density of 2×10^3 cm^{-3} occurred at 260 km. Similarly, it is likely that a solar moderate simulation using the model of *Fox* [2015] would predict the O^+ peak density accurately but at a lower altitude than observed by MAVEN NGIMS. By contrast, *Shinagawa and Cravens* [1992] did predict O^+ peak density and altitude accurately. One possible explanation is that vertical plasma transport is suppressed by a horizontal magnetic field to a greater extent than is assumed in most simulations, which will increase the density and altitude of the O^+ peak.

Seasonal effects may also affect the O^+ peak altitude [*Chaufray et al.*, 2014]. The Viking measurements were acquired at Ls = 97°, near the start of northern summer and near aphelion, under solar minimum conditions, and the MAVEN measurements were acquired at Ls = 299° − 348°, during northern winter and near perihelion, under solar moderate conditions. Both the increase in solar activity and the decrease in Mars-Sun distance from Viking to MAVEN cause greater heating of the lower thermosphere, which expands the atmosphere and

shifts any ionospheric peak located at a fixed pressure level upward. These irradiance changes will also affect the neutral O/CO_2 ratio at a fixed pressure level, with greater irradiance causing a smaller O/CO_2 ratio [*Bougher et al.*, 2000]. Many of the modeling papers discussed in this article used generic neutral atmospheric profiles for a set level of solar activity and did not consider seasonal effects. Moreover, many used an O profile inferred indirectly from Viking Lander observations.

In the MAVEN NGIMS observations, the O^+ ion density increases exponentially with increasing altitude from low altitudes up to its peak and does so with a scale height that is similar to the scale height with which the O_2^+ ion density decreases with increasing altitude. The models of *Shinagawa and Cravens* [1992], *Terada et al.* [2009], and *Dong et al.* [2015] did not predict an exponential increase in the O^+ density with altitude. The models of *Krasnopolsky* [2002], *Chaufray et al.* [2014], and *Fox* [2015] do predict an exponential increase but with a scale height that is not similar to the O_2^+ scale height. By contrast, *Chen et al.* [1978], *Ma et al.* [2004], *Najib et al.* [2011], and *Matta et al.* [2014] did accurately predict an exponential increase in the O^+ ion density with a scale height similar to the O_2^+ scale height.

In the MAVEN NGIMS observations, O^+ and O_2^+ densities were approximately equal above 280 km. The models of *Chen et al.* [1978], *Krasnopolsky* [2002], *Najib et al.* [2011], *Matta et al.* [2014], and *Fox* [2015] predicted a topside composition dominated by O_2^+, while the models of *Shinagawa and Cravens* [1992] and *Terada et al.* [2009] predicted a topside composition dominated by O^+. Even at solar maximum, *Fox* [2015] predicted a topside composition dominated by O_2^+. The model of *Chaufray et al.* [2014] did not extend to high enough altitudes to predict the composition above 300 km. However, this model predicts that the O^+/O_2^+ ratio at a pressure level of 8×10^{-8} Pa varies by an order of magnitude with season. Such possible seasonal effects are not considered in this work. By contrast, the models of *Ma et al.* [2004] and *Dong et al.* [2015] did predict a mixed topside composition.

There are several factors that may have contributed to differences between these compositional predictions and observations. The O^+ density is strongly dependent on the density of neutral O, which was not directly measured by the Viking neutral mass spectrometer [*Nier and McElroy*, 1977] and which is predicted to be highly variable with local time and season [*Valeille et al.*, 2009a, 2009b; *González-Galindo et al.*, 2009a, 2009b]. As noted above, the thermospheric temperature and any inhibition of vertical plasma transport by magnetic fields will also affect the O^+ density. Assumptions about ionospheric temperatures, which affect reaction rates, and about solar wind and crustal magnetic fields may also have contributed.

The models of *Ma et al.* [2004] and *Dong et al.* [2015] successfully predicted several features of the behavior of O^+ and the exponential decrease of ion densities at high altitudes. Yet many aspects of these models are similar to, or even simpler than, the equivalent aspects of many of the other models considered herein. The neutral atmosphere includes only CO_2, O, and H, with H being a minor constituent over most of the altitudes discussed here. The solar irradiance is monochromatic, and the set of chemical reactions is minimal. The model of *Najib et al.* [2011] is closely related to the models of *Ma et al.* [2004] and *Dong et al.* [2015]. Yet the models of *Ma et al.* [2004] and *Dong et al.* [2015] accurately predicted a mixed O^+/O_2^+ topside composition, whereas the model of *Najib et al.* [2011] did not. We defer explanation of this difference to future work.

Since the models of *Ma et al.* [2004] and *Terada et al.* [2009] are both single-fluid MHD models, the differences between their predictions for the same solar zenith angle are noteworthy. *Terada et al.* [2009] predicted that O^+ is the dominant species in the topside ionosphere, which is neither observed nor predicted by *Ma et al.* [2004]. We have not conclusively determined the reasons for these differences, but do note that *Ma et al.* [2004] showed that conditions in the topside ionosphere are not simply a function of solar zenith angle. Geographic location is also important. The location at which the ion density profiles of *Terada et al.* [2009] (Figure 2j) were calculated is not stated by those authors, so it may well differ from the location selected by *Ma et al.* [2004] (Figure 2i).

Relative to other models, the unique attribute of the models of *Ma et al.* [2004] and *Dong et al.* [2015] is their inclusion of three-dimensional plasma transport (MHD) and interactions with the surrounding space environment. It appears that three-dimensional plasma transport driven by interactions with the surrounding space environment plays an important role in controlling the behavior of the major species in the ionosphere of Mars at high altitudes. Yet inclusion of these effects is no guarantee of model success, as demonstrated by *Terada et al.* [2009] and *Najib et al.* [2011].

In order for the MAVEN mission to reach conclusions about the integrated history of the escape of volatiles from Mars from analysis of present-day observations, it will be necessary to validate numerical models under present-day conditions then use them to extrapolate back over billions of years of solar system history. Many of the models described herein are available to the MAVEN team for that activity, and the initial results reported herein will inform decisions about how best to apply these modeling resources to this problem. Another challenge is to simulate and reproduce the neutral and ion densities simultaneously once instrument calibrations are mature. This article has focused on previously published simulations; new simulations based on the conditions appropriate for the MAVEN NGIMS observations will be particularly informative.

Acknowledgments
We acknowledge Francisco Gonzalez-Galindo and an anonymous reviewer. P.W. and M.V. were supported, in part, by NASA award NNX13AO35G. MAVEN data are available from the NASA Planetary Data System (http://pds.nasa.gov). The MAVEN project is supported by NASA through the Mars Exploration Program.

The Editor thanks Francisco Gonzalez-Galindo and an anonymous reviewer for their assistance in evaluating this paper.

References

Benna, M., P. R. Mahaffy, J. M. Grebowsky, J. L. Fox, R. V. Yelle, and B. M. Jakosky (2015), First measurements of composition and dynamics of the Martian ionosphere by MAVEN's Neutral Gas and Ion Mass Spectrometer, *Geophys. Res. Lett.*, *42*, doi:10.1002/2015GL066146.

Bougher, S. W., S. Engel, R. G. Roble, and B. Foster (2000), Comparative terrestrial planet thermospheres: 3. Solar cycle variation of global structure and winds at solstices, *J. Geophys. Res.*, *105*, 17,669–17,692, doi:10.1029/1999JE001232.

Breus, T. K., K. Y. Pimenov, M. N. Izakov, A. M. Krymskii, J. G. Luhmann, and A. J. Kliore (1998), Conditions in the Martian ionosphere/atmosphere from a comparison of a thermospheric model with radio occultation data, *Planet. Space Sci.*, *46*, 367–376, doi:10.1016/S0032-0633(97)00168-2.

Chaufray, J.-Y., F. Gonzalez-Galindo, F. Forget, M. Lopez-Valverde, F. Leblanc, R. Modolo, S. Hess, M. Yagi, P.-L. Blelly, and O. Witasse (2014), Three-dimensional Martian ionosphere model: II. Effect of transport processes due to pressure gradients, *J. Geophys. Res. Planets*, *119*, 1614–1636, doi:10.1002/2013JE004551.

Chen, R. H., T. E. Cravens, and A. F. Nagy (1978), The Martian ionosphere in light of the Viking observations, *J. Geophys. Res.*, *83*, 3871–3876.

Dong, C., S. W. Bougher, Y. Ma, G. Toth, Y. Lee, A. F. Nagy, V. Tenishev, D. J. Pawlowski, M. R. Combi, and D. Najib (2015), Solar wind interaction with the Martian upper atmosphere: Crustal field orientation, solar cycle and seasonal variations, *J. Geophys. Res. Space Physics*, doi:10.1002/2015JA020990.

Forget, F., F. Hourdin, R. Fournier, C. Hourdin, O. Talagrand, M. Collins, S. R. Lewis, P. L. Read, and J.-P. Huot (1999), Improved general circulation models of the Martian atmosphere from the surface to above 80 km, *J. Geophys. Res.*, *104*, 24,155–24,176, doi:10.1029/1999JE001025.

Fox, J. L. (2015), The chemistry of protonated species in the Martian ionosphere, *Icarus*, *252*, 366–392, doi:10.1016/j.icarus.2015.01.010.

González-Galindo, F., F. Forget, M. A. López-Valverde, M. Angelats i Coll, and E. Millour (2009a), A ground-to-exosphere Martian general circulation model: 1. Seasonal, diurnal, and solar cycle variation of thermospheric temperatures, *J. Geophys. Res.*, *114*, E04001, doi:10.1029/2008JE003246.

González-Galindo, F., F. Forget, M. A. López-Valverde, and M. Angelats i Coll (2009b), A ground-to-exosphere Martian general circulation model: 2. Atmosphere during solstice conditions—Thermospheric polar warming, *J. Geophys. Res.*, *114*, E08004, doi:10.1029/2008JE003277.

González-Galindo, F., J.-Y. Chaufray, M. A. López-Valverde, G. Gilli, F. Forget, F. Leblanc, R. Modolo, S. Hess, and M. Yagi (2013), Three-dimensional Martian ionosphere model: I. The photochemical ionosphere below 180 km, *J. Geophys. Res. Planets*, *118*, 2105–2123, doi:10.1002/jgre.20150.

Hanson, W. B., S. Sanatani, and D. R. Zuccaro (1977), The Martian ionosphere as observed by the Viking retarding potential analyzers, *J. Geophys. Res.*, *82*, 4351–4363.

Krasnopolsky, V. A. (2002), Mars' upper atmosphere and ionosphere at low, medium, and high solar activities: Implications for evolution of water, *J. Geophys. Res.*, *107*(E12), 5128, doi:10.1029/2001JE001809.

Ma, Y., A. F. Nagy, I. V. Sokolov, and K. C. Hansen (2004), Three-dimensional, multispecies, high spatial resolution MHD studies of the solar wind interaction with Mars, *J. Geophys. Res.*, *109*, A07211, doi:10.1029/2003JA010367.

Mahaffy, P. R., et al. (2014), The neutral gas and ion mass spectrometer on the Mars atmosphere and volatile evolution mission, *Space Sci. Rev.*, doi:10.1007/s11214-014-0091-1, in press.

Matta, M., P. Withers, and M. Mendillo (2013), The composition of Mars' topside ionosphere: Effects of hydrogen, *J. Geophys. Res. Space Physics*, *118*, 2681–2693, doi:10.1002/jgra.50104.

Matta, M., M. Galand, L. Moore, M. Mendillo, and P. Withers (2014), Numerical simulations of ion and electron temperatures in the ionosphere of Mars: Multiple ions and diurnal variations, *Icarus*, *227*, 78–88, doi:10.1016/j.icarus.2013.09.006.

Najib, D., A. F. Nagy, G. Tóth, and Y. Ma (2011), Three-dimensional, multifluid, high spatial resolution MHD model studies of the solar wind interaction with Mars, *J. Geophys. Res.*, *116*, A05204, doi:10.1029/2010JA016272.

Nier, A. O., and M. B. McElroy (1977), Composition and structure of Mars' upper atmosphere—Results from the neutral mass spectrometers on Viking 1 and 2, *J. Geophys. Res.*, *82*, 4341–4349.

Shinagawa, H., and T. E. Cravens (1989), A one-dimensional multispecies magnetohydrodynamic model of the dayside ionosphere of Mars, *J. Geophys. Res.*, *94*, 6506–6516.

Shinagawa, H., and T. E. Cravens (1992), The ionospheric effects of a weak intrinsic magnetic field at Mars, *J. Geophys. Res.*, *97*, 1027–1035.

Terada, N., Y. N. Kulikov, H. Lammer, H. I. M. Lichtenegger, T. Tanaka, H. Shinagawa, and T. Zhang (2009), Atmosphere and water loss from early Mars under extreme solar wind and extreme ultraviolet conditions, *Astrobiology*, *9*, 55–70, doi:10.1089/ast.2008.0250.

Valeille, A., V. Tenishev, S. W. Bougher, M. R. Combi, and A. F. Nagy (2009a), Three-dimensional study of Mars upper thermosphere/ionosphere and hot oxygen corona: 1. General description and results at equinox for solar low conditions, *J. Geophys. Res.*, *114*, E11005, doi:10.1029/2009JE003388.

Valeille, A., M. R. Combi, S. W. Bougher, V. Tenishev, and A. F. Nagy (2009b), Three-dimensional study of Mars upper thermosphere/ionosphere and hot oxygen corona: 2. Solar cycle, seasonal variations, and evolution over history, *J. Geophys. Res.*, *114*, E11006, doi:10.1029/2009JE003389.